MIKAILALSYS
Journal of Multidisciplinary Sciences

e-ISSN : 2987-2286
p-ISSN : 2987-3924

Index: Harvard, Boston, Sydney, Copernicus, Sinta 4, Scilit, Semantic, Google, etc

https://doi.org/10.58578/mikailalsys.v4i3.11957

Flood-Prone Area Mapping Using the Integration of Hydrological Data and Google Earth Engine (GEE)

Firman Pindria & Jonni Mardizal
Universitas Negeri Padang, Indonesia
firmanpindria1122@gmail.com; jonni.mardizal@ft.unp.ac.id

Article Info:

Submitted:	Revised:	Accepted:	Published:
Jul 17, 2026	Aug 14, 2026	Aug 26, 2026	Aug 31, 2026

Abstract

Flood susceptibility mapping that integrates hydrological and geospatial information remains limited at the sub-watershed scale, particularly in rapidly developing coastal urban areas. This study maps flood susceptibility in the Batang Kandis Sub-watershed, Padang City, by integrating hydrological data through Google Earth Engine (GEE). A quantitative spatial approach was employed using six parameters: rainfall, elevation, slope, soil texture, land cover, and proximity to rivers. Each parameter was classified, scored, and weighted using the Analytic Hierarchy Process (AHP), after which a weighted overlay was applied to generate the Flood Susceptibility Index (FSI). The results indicate that 58.77% of the study area is classified as having very high flood susceptibility, while 21.39% is classified as highly susceptible. These zones are concentrated primarily in downstream areas characterized by low elevations, gentle slopes, extensive built-up surfaces, and close proximity to river networks. Validation against historical inundation data from Ina-Geoportal demonstrated 97.10% spatial correspondence with areas classified as having high or very high susceptibility. These findings confirm that integrating hydrological and geospatial parameters through GEE provides a reliable approach to identifying flood-prone areas at the sub-watershed scale. The resulting susceptibility map

Mikailalsys is licensed under a Creative Commons Attribution-NonCommercial-ShareAlike 4.0 International License

provides an evidence-based foundation for prioritizing flood mitigation, strengthening watershed management, and supporting adaptive spatial planning in rapidly developing coastal urban areas.

Keywords: Batang Kandis Sub-Watershed; Flood Susceptibility; Flood Susceptibility Index; Google Earth Engine; Hydrological Data

INTRODUCTION

Flooding remains one of the most persistent hydrometeorological hazards affecting communities across different regions of the world (Akram & Mushtaq, 2024; Barendrecht et al., 2024; Shah et al., 2025; Sibandze et al., 2025). Its consequences extend beyond physical inundation, often disrupting livelihoods, damaging infrastructure, displacing residents, and placing additional pressure on local economies and public services (Andayono et al., 2024; Geospasial, 2026; Nurpasari & Febriamansyah, 2020). Recent global climate assessments indicate that extreme weather events, including floods, continue to produce substantial social and economic losses as the climate system becomes increasingly variable (Organization, 2025). Flood impacts are also closely related to the interaction between natural hydrological processes and human activities, particularly where settlements and infrastructure continue to expand into areas with limited capacity to accommodate excess water. This condition places flood risk not merely as a hydrological concern, but also as an issue of environmental management, spatial planning, and community resilience.

Flood occurrence in Indonesia reflects a similarly complex interaction among rainfall, watershed characteristics, river capacity, land-cover change, and urban development. Kodoatie & Sjarief (2010) describe flooding as a condition in which water discharge exceeds the carrying capacity of a river or drainage system, allowing water to spread into surrounding areas. From a watershed perspective, Asdak (2010) explains that high rainfall intensity can generate substantial surface runoff when precipitation exceeds the infiltration capacity of the soil. Changes in land use may intensify this process by reducing permeable surfaces and altering the natural response of a catchment to rainfall. Nugroho & Handayan (2021) similarly demonstrate that flood problems cannot be separated from the interaction between drainage systems, river conditions, and broader spatial development. Flooding in Indonesia therefore needs to be understood through a spatially integrated perspective rather than through rainfall or river discharge as isolated variables.

Padang City represents a particularly relevant setting for such an approach because its rapidly developing urban landscape is situated within a coastal environment influenced by several river and sub-watershed systems. Flood events in 2025 demonstrated the scale of this vulnerability. Records from the Badan Penanggulangan Bencana Daerah Kota Padang (BPBD Kota Padang, 2025) reported 31,845 people affected, eight fatalities, and 17,220 residents displaced, with Koto Tangah District accounting for the largest number of affected residents. Infrastructure damage associated with the same hydrometeorological disaster was estimated at approximately IDR 202.8 billion (Padang, 2025). Spatial disaster information maintained by the Badan Informasi Geospasial Bumi & Rezagama (2023) further provides evidence that flood-affected areas are distributed across parts of Padang and the surrounding watershed system. These impacts show that flood mapping in Padang carries immediate practical relevance because the resulting information concerns not only physical landscapes, but also communities whose safety, mobility, and livelihoods depend on more responsive disaster-risk planning.

The Batang Kandis Sub-watershed is one of the hydrological units associated with flood-prone areas in northern Padang, particularly Koto Tangah District. Its landscape ranges from relatively elevated terrain in the upstream section to increasingly developed areas and low-lying floodplains toward the downstream zone. Such spatial variation influences the way rainfall is transformed into infiltration, surface runoff, and river flow. Arsyad (2010) considers a sub-watershed an important hydrological observation unit because its physical characteristics directly influence the quantity and quality of flow entering the main river system. Changes in slope, soil properties, land cover, and rainfall distribution can consequently alter runoff generation and increase the likelihood of flooding downstream. The hydrological meaning of these variables becomes especially important in an urbanizing sub-watershed, where the conversion of water-absorbing surfaces into built-up areas may gradually reduce the capacity of the landscape to moderate storm runoff (Bumi & Rezagama, 2023).

Reliable identification of flood-prone areas requires spatial information that can represent these interacting controls over a sufficiently broad area and at a level of detail useful for planning. Conventional geospatial processing can become demanding when rainfall, elevation, soil, land-cover, and river-network datasets originate from different sources and require repeated preprocessing. Google Earth Engine (GEE) offers an alternative through cloud-based access to large geospatial archives and scalable computational resources.

Gorelick et al. (2017) describe GEE as a planetary-scale geospatial analysis platform designed to facilitate efficient and reproducible processing of extensive Earth observation datasets. Its data environment allows hydrological and environmental information to be brought together, including CHIRPS precipitation products Geospasial (2026) , Sentinel-1 radar imagery and Sentinel-2 multispectral imagery (European Space Agency [ESA], 2024a, 2024b), and Shuttle Radar Topography Mission elevation data (National Aeronautics and Space Administration [NASA] & United States Geological Survey (Saifurridzal & Sakinah, 2022). Soil information derived from globally available soil datasets can further support the representation of infiltration-related characteristics within susceptibility analysis (Hengl, 2018).

Previous studies have demonstrated the value of GEE for flood analysis in different Indonesian environments, although their analytical emphases vary considerably. Saifurridzal & Sakinah (2022) used GEE, Sentinel-1, and elevation information to identify flood-safe zones in the coastal area of Jember Regency. Sugandhi & Rakuasa (2023) incorporated variables such as elevation, distance from rivers, vegetation condition, and topographic position to analyze flood susceptibility in Jakarta. Pratama et al. (2024) applied GEE to investigate the spatial and temporal characteristics of extreme rainfall associated with flooding in Kampar Regency using CHIRPS data. More recently, Irfan et al. (2025) mapped flood occurrence in Pekanbaru using Sentinel-1 SAR data and a locally calibrated threshold, with flood-distribution results compared against records from relevant water-resource and disaster-management agencies. These studies confirm that GEE can reduce computational constraints and facilitate flood-related spatial analysis across areas with different environmental settings.

The growing sophistication of cloud-based flood mapping also reveals an important methodological issue. Recent work has moved toward increasingly automated flood-detection systems that combine Sentinel-1 SAR imagery, topographic information, and cloud computing to generate rapid flood products (Tian et al., 2026). Such developments are valuable for detecting where inundation has occurred, yet event-based flood extraction and long-term flood susceptibility mapping do not address exactly the same question. Studies in Indonesia have frequently concentrated on observed inundation during particular events, temporal rainfall characteristics, safe-zone delineation, or susceptibility assessments based on selected geospatial indicators (Irfan et al., 2025; Pratama et al., 2024; Saifurridzal & Sakinah, 2022; Sugandhi & Rakuasa, 2023). A practical gap therefore remains in integrating

hydrologically meaningful environmental variables within a cloud-based susceptibility framework and subsequently examining whether the resulting susceptibility pattern corresponds to actual inundation evidence in a relatively small, rapidly developing tropical sub-watershed.

The contribution of the present study lies in addressing this gap through a distinction between factors that explain flood susceptibility and data that record actual flood conditions. Rainfall information derived from CHIRPS represents the spatial distribution of precipitation, while elevation and slope derived from SRTM describe the topographic control on water movement. Soil characteristics provide information related to infiltration potential, and Sentinel-2 imagery supports the representation of land-cover conditions that influence surface runoff (Group, 2023; Hengl, 2018; Organization, 2025). River proximity is considered because areas closer to drainage channels may experience different levels of exposure to river overflow. Sentinel-1 SAR imagery, by contrast, is used as supporting evidence for identifying actual inundation because radar observations remain useful under cloudy weather conditions (Agency, 2024b, 2024a). The novelty of this research consequently does not rest on the use of GEE alone, but on the integration of hydrological reasoning, multi-source geospatial parameters, cloud-based processing, and spatial evaluation against observed flood inundation within the specific environmental context of the Batang Kandis Sub-watershed.

This study aims to map flood-prone areas in the Batang Kandis Sub-watershed, Padang City, by integrating hydrological and geospatial data through Google Earth Engine. The analysis is designed to identify the spatial distribution of different flood-susceptibility levels by considering rainfall, topography, soil characteristics, land cover, and proximity to the river network, while Sentinel-1-derived inundation information and available disaster records are used to examine the spatial consistency of the resulting map. The study is expected to provide a more locally grounded representation of flood susceptibility that can support disaster mitigation, watershed management, infrastructure planning, and more adaptive spatial development in Padang City. Its broader contribution is to demonstrate how cloud-based geospatial technology can be connected with hydrological understanding to produce information that is not only technically reproducible, but also more meaningful for communities and institutions living with recurring flood risk.

METHODS

This study employed an applied quantitative-spatial approach to produce a flood susceptibility map for the Batang Kandis Sub-watershed in Padang City, West Sumatra. A case-study design was adopted because the analysis focused on a specific hydrological unit with distinct topographic, land-cover, soil, and drainage characteristics. Quantitative spatial analysis was considered appropriate because the study converted environmental and hydrological conditions into measurable raster-based variables that could be classified, scored, weighted, and spatially integrated. The analytical unit consisted of all valid terrestrial pixels within the Batang Kandis Sub-watershed rather than a conventional human population or respondent sample. Accordingly, no probabilistic sampling was applied; all pixels containing complete information for the six susceptibility parameters were included in the analysis. This approach is consistent with quantitative research, in which measurable variables are systematically examined to identify patterns and relationships within a defined analytical framework (Creswell, 2014). Google Earth Engine (GEE) served as the principal cloud-computing environment because it enables large geospatial datasets to be accessed, processed, and integrated efficiently within a reproducible workflow (Gorelick et al., 2017).

The data were predominantly secondary and were obtained from official geospatial repositories and global Earth-observation datasets. Six parameters were used to construct the Flood Susceptibility Index (FSI): mean annual rainfall derived from CHIRPS Daily data for 2016–2025; elevation from the Shuttle Radar Topography Mission (SRTM) Digital Elevation Model; slope derived from SRTM; surface soil texture from the OpenLandMap USDA Soil Texture dataset; 2025 land cover derived from Dynamic World; and Euclidean distance from the river network extracted from MERIT Hydro. Supporting flood-event information from BPBD Kota Padang and flood polygons from the Ina-Geoportal of the Badan Informasi Geospasial were used for spatial validation. Before integration, all spatial layers were clipped to the same Region of Interest, referenced to WGS 84/UTM Zone 47S (EPSG:32747), and aligned to a common 30 m analysis grid. The 30 m grid represents the analytical output resolution and does not imply that all source datasets originally had the same spatial resolution. Categorical soil-texture data were resampled using the nearest-neighbor method to preserve the original USDA classes, while land-cover classes were derived from annual mean Dynamic World class probabilities. Water bodies were masked from the terrestrial susceptibility analysis to avoid assigning flood-susceptibility scores to permanent water surfaces.

Data analysis consisted of reclassification, parameter weighting, weighted overlay, FSI classification, area estimation, and spatial validation. Each parameter was transformed into a susceptibility score ranging from 1 to 5, where higher scores represented a greater contribution to flood susceptibility. Parameter weights were determined using the Analytic Hierarchy Process (AHP), assigning weights of 25% to rainfall, 20% to elevation, 15% to slope, 10% to soil texture, 10% to land cover, and 20% to river proximity. The final index was calculated using the weighted linear combination (FSI=\sum_{i=1}^{6} w_i s_i), where (w_i) represents the weight of each parameter and (s_i) represents its reclassified susceptibility score. The resulting FSI values were grouped into five classes very low, low, moderate, high, and very high using intervals of 1.00–1.80, >1.80–2.60, >2.60–3.40, >3.40–4.20, and >4.20–5.00, respectively. Class areas and percentages were subsequently calculated using pixel-area statistics in GEE. Model performance was evaluated through spatial overlay between the resulting susceptibility map and observed flood polygons from Ina-Geoportal, with the proportion of recorded inundated areas falling within the higher-susceptibility classes used to assess spatial agreement. Google Earth Engine was used for raster processing and weighted-overlay analysis, while QGIS supported map layout, spatial overlay, and final cartographic presentation.

RESULTS

1. Study Area Characteristics

The Batang Kandis Sub-watershed covers approximately 33.49 km² in Koto Tangah District, Padang City, West Sumatra. Its physical setting is characterized by a clear upstream–downstream contrast, with relatively elevated and steep terrain in the eastern upstream section and an extensive low-lying coastal plain toward the western downstream area. This configuration creates a natural pathway for surface runoff to move from the upper catchment toward the lower part of the watershed, where residential and built-up areas have expanded considerably.

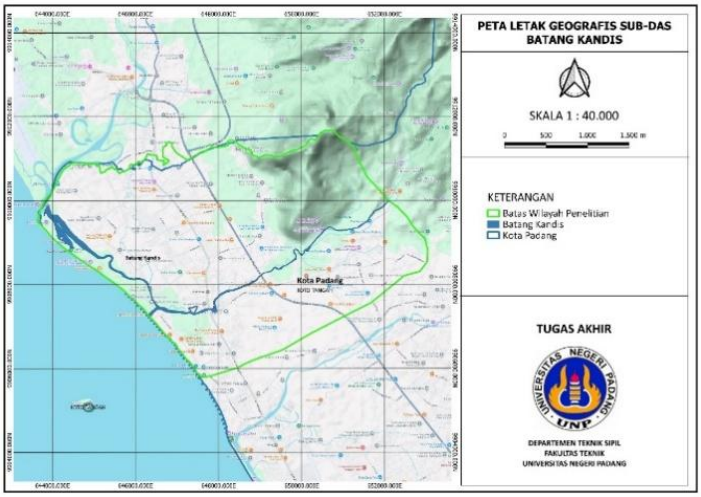


Figure 1. Geographic Location of the Batang Kandis Sub-watershed

Figure 1 presents the geographical location of the Batang Kandis Sub-watershed and illustrates its position within the broader administrative area of Koto Tangah District. Spatial processing identified 32.202 km² of terrestrial area that could be consistently analyzed after permanent water bodies and unmapped boundary pixels were excluded. The permanent water-body area accounted for 0.856 km², while approximately 0.43 km² remained unmapped because of incomplete raster coverage along the watershed boundary. A total of 35,776 terrestrial pixels contained complete information for all six flood-susceptibility parameters and were therefore retained for the final Flood Susceptibility Index (FSI) calculation.

2. Rainfall Characteristics

Table 1. Annual Rainfall in the Batang Kandis Sub-watershed, 2016–2025

Year	Mean Annual Rainfall (mm)
2016	3,958
2017	4,051
2018	3,808
2019	3,024
2020	3,827
2021	4,050
2022	4,522
2023	3,521
2024	4,031
2025	4,169
Ten-year mean	3,896

The annual distribution is summarized in Table 1. Rainfall analysis using CHIRPS data for 2016–2025 showed considerable interannual variation across the Batang Kandis

Sub-watershed. Annual rainfall ranged from 3,024 mm in 2019 to 4,522 mm in 2022, with a ten-year mean of approximately 3,896 mm/year. Annual rainfall remained above 4,000 mm in several years, including 2017, 2021, 2022, 2024, and 2025.

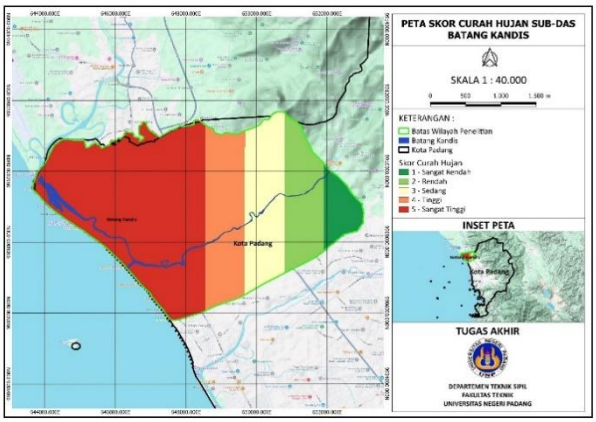


Figure 2. Spatial Distribution and Reclassified Scores of Mean Annual Rainfall in the Batang Kandis Sub-watershed

The spatial rainfall surface presented in Figure 2 indicates that the mean annual rainfall across the study area ranged from approximately 3,636.40 mm/year to more than 3,908.42 mm/year. Areas classified in the highest rainfall-susceptibility score were widely distributed from the eastern upstream sector toward the central part of the watershed. The rainfall pattern therefore indicates that a substantial portion of the catchment is consistently exposed to high precipitation input, which provides a strong hydrological contribution to runoff generation during intense rainfall periods.

3. Topographic Characteristics

Table 2. Distribution of Elevation Classes in the Batang Kandis Sub-watershed

Elevation (m)	Susceptibility Level	Score	Area (km²)	Percentage (%)
<25	Very high	5	26.81	80.44
25–<50	High	4	2.47	7.41
50–<100	Moderate	3	1.24	3.71
100–200	Low	2	1.31	3.93
>200	Very low	1	1.50	4.51
Total	—	—	33.34	100.00

Based on table 2 Elevation analysis based on SRTM DEM revealed a marked dominance of low-lying terrain. Elevation ranged from approximately 0 to 476 m above sea level, with a mean elevation of only 28.2 m. As presented in Table 2, 26.81 km², equivalent to 80.44% of the mapped area, lies below 25 m above sea level and was assigned the highest

flood-susceptibility score. Areas above 100 m account for less than 9% of the watershed and are primarily concentrated in the eastern upstream zone.

Table 3. Distribution of Slope Classes in the Batang Kandis Sub-watershed

Slope (%)	Terrain Character	Susceptibility Level	Score	Area (km²)	Percentage (%)
0–8	Flat	Very high	5	21.21	63.61
>8–15	Gentle	High	4	6.84	20.52
>15–25	Moderately steep	Moderate	3	1.86	5.59
>25–40	Steep	Low	2	1.74	5.22
>40	Very steep	Very low	1	1.69	5.06
Total	—	—	—	33.34	100.00

Based on table 3 Slope analysis produced a similar spatial pattern. Flat terrain with slopes of 0–8% occupied 21.21 km² or 63.61% of the mapped area, while gently sloping terrain of >8–15% accounted for another 20.52%. More than 84% of the landscape can therefore be characterized as flat to gently sloping. Steeper slopes were confined mainly to the upstream section.

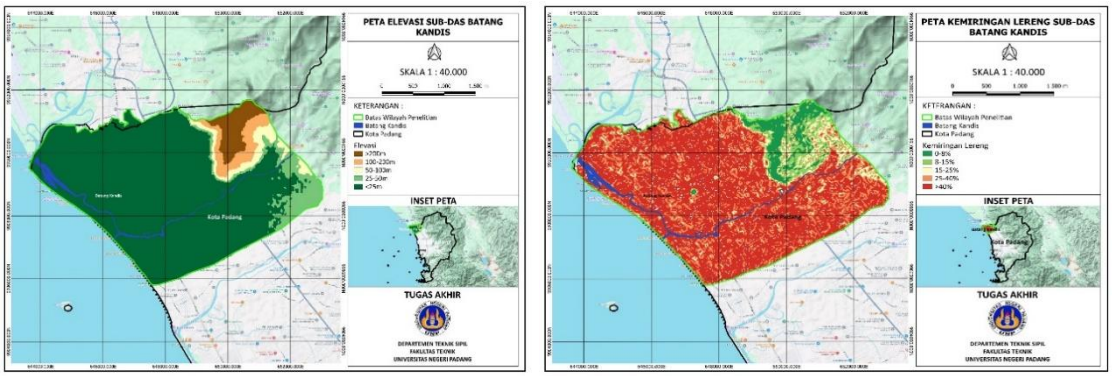


Figure 3. Elevation and Slope Distribution in the Batang Kandis Sub-watershed

Figure 3 illustrates the strong spatial transition from steep upper catchment areas to extensive flat terrain in the central and downstream parts of the watershed. The combination of low elevation and gentle slopes is particularly evident in the western downstream sector. This area receives flow generated from the higher eastern catchment while simultaneously offering relatively limited topographic gradients for rapid drainage. The spatial coincidence of these two conditions produces extensive zones in which water can accumulate or remain on the surface for longer periods.

The combination of low elevation and gentle slopes is particularly evident in the western downstream sector. This area receives flow generated from the higher eastern catchment while simultaneously offering relatively limited topographic gradients for rapid

drainage. The spatial coincidence of these two conditions produces extensive zones in which water can accumulate or remain on the surface for longer periods.

4. Texture, Land Cover, and River Proximity

Table 4. Distribution of Land-Cover Classes

Land-Cover Class	Susceptibility Score	Area (km²)	Percentage (%)
Forest/tree cover	1	13.27	39.81
Shrub, grass, and garden	2	0.49	1.46
Agriculture/wetland	3	3.86	11.56
Bare land	4	0.16	0.49
Built-up area	5	14.74	44.22
Terrestrial classes represented	—	32.52	97.55

Based on table 4 land-cover analysis using Dynamic World for 2025 revealed a contrasting landscape structure between built-up areas and forest cover. Built-up areas represented the largest individual class, covering 14.74 km² or 44.22% of the mapped terrestrial surface. Forest and tree cover occupied 13.27 km² or 39.81%. Agricultural and wetland areas accounted for 3.86 km² or 11.56%, whereas shrubland, grassland, gardens, and bare land represented relatively small proportions. Built-up areas were strongly concentrated in the central and downstream sections of the watershed, whereas forest cover remained predominantly in the eastern upstream zone.

Permanent water bodies were excluded from the land-based weighted-overlay calculation. This separation ensured that existing river channels and permanently inundated surfaces were not interpreted as terrestrial areas susceptible to future flooding.



Figure 4. Spatial Distribution of (a) Soil Texture, (b) Land Cover, and (c) Distance from the River Network

The spatial distribution of the soil classes is shown in Figure 4a. Soil texture analysis showed that the study area is dominated by relatively fine-textured soils. Clay loam covered 21.84 km² or 65.53% of the analyzed area, while clay accounted for another 9.15 km² or

27.44%. Together, these two classes represented more than 90% of the mapped soil area. Sandy clay loam and sandy clay occupied much smaller proportions.

5. Flood Susceptibility Index

The six standardized parameters were integrated using the AHP-derived weights and weighted-overlay procedure. Rainfall received the largest weight at 25%, followed by elevation and river proximity at 20% each, slope at 15%, and soil texture and land cover at 10% each. The weighted combination generated continuous FSI values for all 35,776 valid terrestrial pixels.

Table 5. Descriptive Statistics of the Flood Susceptibility Index

Statistic	Value
Minimum	1.300
Maximum	5.000
Mean	4.028
Standard deviation	0.822
Valid pixels	35,776

The statistical distribution of the resulting FSI is presented in Table 5. Index values ranged from 1.30 to 5.00, with a mean of 4.028 and a standard deviation of 0.822. Based on the predetermined classification thresholds, the mean value falls within the high susceptibility interval (>3.40–4.20), indicating that the overall physical setting of the analyzed terrestrial area tends toward the upper end of the susceptibility spectrum.

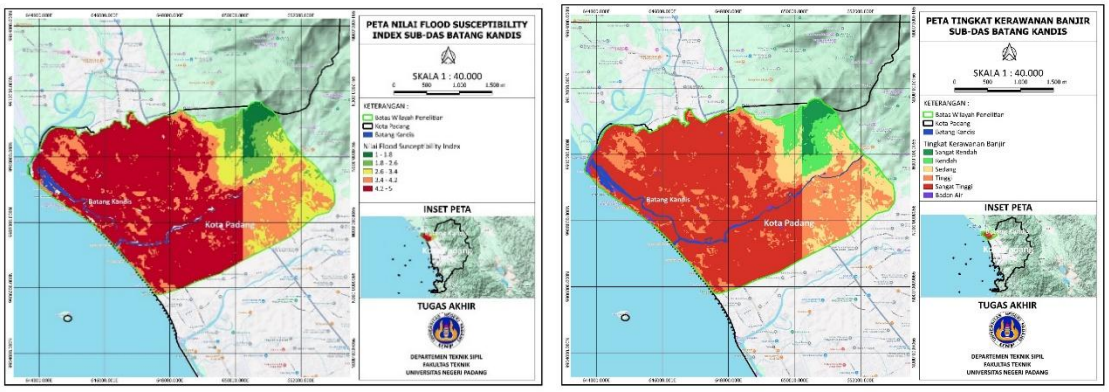


Figure 5. Flood Susceptibility Index and Flood Susceptibility Classes of the Batang Kandis Sub-watershed

Figure 5 presents the continuous FSI surface and its classification into five susceptibility levels. The resulting pattern is clearly structured rather than randomly distributed. Higher FSI values are concentrated mainly across the middle and downstream portions of the watershed, whereas lower values occur primarily in the eastern upstream area.

6. Distribution of Flood Susceptibility Classes

The final classification demonstrates that most of the analyzed terrestrial area falls within the high and very high susceptibility categories. The very high class occupies 18.926 km² or 58.77% of the study area, making it the dominant category. The high susceptibility class covers 6.889 km² or 21.39%. Taken together, these two classes account for 80.16**%** of the analyzed terrestrial area.

Table 6. Distribution of Flood Susceptibility Classes

Susceptibility Level	FSI Interval	Area (km²)	Percentage (%)
Very low	1.00–1.80	0.781	2.43
Low	>1.80–2.60	1.889	5.87
Moderate	>2.60–3.40	3.717	11.54
High	>3.40–4.20	6.889	21.39
Very high	>4.20–5.00	18.926	58.77
Total	—	32.202	100.00

Based on table 6 the moderate category covers 3.717 km² or 11.54%, while low and very low susceptibility areas comprise only 1.889 km² (5.87%) and 0.781 km² (2.43%), respectively.

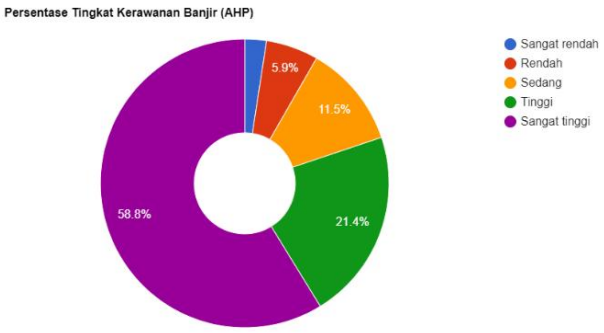


Figure 6. Area Distribution of Flood Susceptibility Classes

Figure 6 shows the proportional distribution of these five classes and highlights the strong dominance of the very high susceptibility category. The spatial pattern shown in Figure 5 demonstrates a clear upstream–downstream differentiation. Very high susceptibility areas are concentrated across the central and western downstream portions of the sub-watershed. These zones spatially coincide with low elevations, flat terrain, developed land cover, and sections located close to the main river channel. Lower susceptibility classes occur primarily toward the eastern upstream area, where higher elevation, steeper terrain, and

relatively extensive forest cover generate lower combined FSI values. The resulting map should therefore be interpreted as a representation of physical flood susceptibility, rather than comprehensive flood risk, because socioeconomic exposure, population vulnerability, infrastructure losses, and institutional coping capacity were not included in the index.

7. Spatial Validation of the Flood Susceptibility Map

Spatial validation was performed by overlaying the FSI map with historical flood-inundation polygons obtained from Ina-Geoportal.

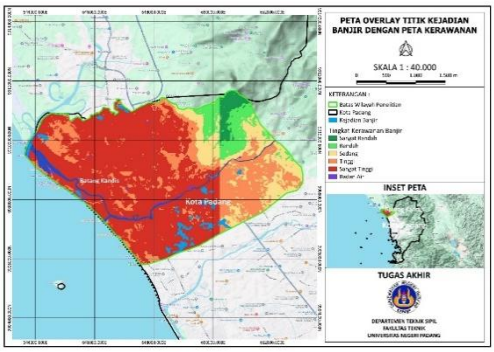


Figure 7. Spatial Overlay of Historical Flood Inundation and the Flood Susceptibility Map

Figure 7 illustrates the spatial correspondence between recorded flood areas and the five modeled susceptibility classes. A total historical inundation area of 69.54 ha was identified within the study area.

Table 7. Spatial Validation of the Flood Susceptibility Map

FSI Class	Susceptibility Level	Historical Inundation Area (ha)	Spatial Correspondence (%)
1	Very low	0.00	0.00
2	Low	0.00	0.00
3	Moderate	2.01	2.89
4	High	8.15	11.72
5	Very high	59.38	85.38
Total	—	69.54	100.00

Based on table 7 the validation results show that 59.38 ha, equivalent to 85.38% of the recorded inundation area, occurred within the very high susceptibility class. Another 8.15 ha or 11.72% was located within the high susceptibility class, while only 2.01 ha or 2.89% occurred in the moderate class. No recorded inundation polygons were identified within the low or very low susceptibility zones.

The combined proportion of historical inundation occurring within the high and very high susceptibility classes reached 97.10**%**. This strong spatial correspondence indicates that

the susceptibility model successfully concentrated most historically flooded areas within the two upper susceptibility categories. The remaining 2.89% of inundated area occurring in the moderate class suggests that localized factors not explicitly represented by the six model parameters may also contribute to flooding at particular sites. Such factors may include local drainage conditions, channel sedimentation, culvert capacity, or other small-scale hydrological modifications. Overall, the validation provides empirical support for the spatial pattern generated by the integrated hydrological–GEE approach and indicates that the resulting map can serve as a useful biophysical baseline for flood mitigation and spatial planning in the Batang Kandis Sub-watershed.

DISCUSSION

The spatial pattern produced by the Flood Susceptibility Index (FSI) indicates that flood susceptibility in the Batang Kandis Sub-watershed is shaped by the combined influence of rainfall, topography, soil properties, land cover, and proximity to the river network rather than by a single dominant factor. More than 80% of the analyzed terrestrial area was classified as having high or very high flood susceptibility, with the highest classes concentrated mainly in the central and downstream portions of the sub-watershed. This distribution is hydrologically meaningful because the downstream landscape combines several unfavorable characteristics: low elevation, relatively flat terrain, fine-textured soils, extensive built-up surfaces, and direct proximity to the Batang Kandis river system. The resulting map therefore captures a clear upstream–downstream contrast, in which runoff generated across the catchment tends to converge toward densely developed lowlands before reaching the coastal outlet.

Rainfall provides an important explanation for this pattern. The CHIRPS dataset for 2016–2025 showed a mean annual rainfall of approximately 3,896 mm/year, with annual totals exceeding 4,000 mm in several years. From a hydrological perspective, rainfall becomes an effective flood-generating mechanism when the amount and intensity of precipitation exceed soil infiltration capacity and the conveyance capacity of drainage and river systems. This interpretation is consistent with Asdak (2010) and (Chow et al., 1988), who explain the close relationship between precipitation, infiltration, runoff production, and river discharge. The findings also correspond with Pratama et al. (2024) , who demonstrated the usefulness of CHIRPS and GEE for examining the spatial and temporal characteristics of rainfall associated with flooding in Kampar Regency. The Batang Kandis case extends this

perspective by showing that rainfall exposure becomes more consequential when it occurs within a landscape already characterized by limited infiltration and extensive low-lying terrain.

Topography further strengthens the downstream concentration of flood susceptibility. Approximately 80.44% of the mapped area lies below 25 m above sea level, while 63.61% consists of terrain with slopes between 0 and 8%. These two conditions create a physical setting in which water arriving from the upper catchment can lose velocity and accumulate over a relatively broad coastal plain. Higher and steeper terrain in the eastern upstream area functions differently: water is less likely to remain locally ponded, although runoff generated there may contribute to discharge farther downstream. A comparable role of topographic configuration has been reported in previous flood-mapping studies. Saifurridzal & Sakinah (2022), for example, identified low-slope coastal areas connected to watershed systems as important flood-prone zones in Jember, while Sugandhi & Rakuasa (2023) incorporated elevation and distance from rivers among the principal spatial variables used to assess flood susceptibility in Jakarta. The similarity across these contrasting study areas suggests that low elevation and gentle slopes remain important physical controls on flood accumulation, although their effects depend on the surrounding watershed and urban context.

Soil texture and land-cover conditions provide another layer of explanation for the high FSI values found in the lower Batang Kandis Sub-watershed. Clay loam and clay collectively dominate more than 90% of the mapped soil area, suggesting that much of the catchment has relatively limited infiltration compared with coarse-textured soils. The prevalence of fine soil textures becomes particularly important when combined with the 44.22% share of built-up land identified from the 2025 land-cover analysis. Roads, roofs, paved yards, and other impervious surfaces interrupt natural infiltration pathways and facilitate the rapid conversion of rainfall into surface runoff. This interaction between physical soil properties and land-use transformation is consistent with the watershed perspective described by Asdak (2010) and with the findings of Nugroho & Handayani (2021), who emphasized that flood occurrence reflects not only hydrological conditions but also drainage performance and spatial development. The Batang Kandis results suggest that urban expansion in downstream areas deserves particular attention because development is occurring precisely where the natural landscape already favors water accumulation.

River proximity adds a distinctly fluvial component to the susceptibility pattern. Areas within 300 m of the extracted river network account for a smaller proportion of the entire sub-watershed than areas farther away, yet many of these zones coincide with densely developed downstream settlements. Their importance is therefore not determined by area alone. When upstream rainfall increases river discharge beyond channel capacity, locations immediately adjacent to the river become the first terrestrial surfaces exposed to overtopping. The linear concentration of high and very high FSI values along parts of the Batang Kandis corridor supports this mechanism. Similar attention to river-related spatial controls appears in the flood susceptibility analysis of Sugandhi & Rakuasa (2023) while Kuswardhana et al. (2023) demonstrated that geospatial approaches can combine physical hazard information with other spatial dimensions to improve flood-related decision making. The present study remains deliberately focused on physical susceptibility rather than broader disaster risk, but the river-corridor pattern provides a useful foundation for subsequent exposure and vulnerability assessments.

The weighted integration of the six parameters produced an FSI distribution in which the very high susceptibility class alone covered 58.77% of the terrestrial analysis area, while the high class represented an additional 21.39%. These proportions are substantially higher than would be expected if unfavorable physical conditions were distributed independently across the landscape. Their spatial overlap indicates that several flood-promoting conditions occur in the same places. Rainfall received the highest AHP weight of 25%, followed by elevation and river proximity at 20% each, while slope, soil texture, and land cover contributed the remaining weights. The importance of this result lies less in the numerical weighting itself than in the way the parameters converge spatially. A low-lying downstream pixel, for example, may simultaneously experience high rainfall, flat terrain, fine-textured soil, built-up cover, and close proximity to a river. Such cumulative physical conditions explain why susceptibility becomes strongly concentrated rather than evenly distributed throughout the watershed.

The validation results provide additional empirical support for this interpretation. Of the 69.54 ha of historical inundation identified from Ina-Geoportal, 59.38 ha or 85.38% occurred within the very high susceptibility class, while another 8.15 ha or 11.72% occurred within the high class. The combined spatial correspondence of historical inundation with these two classes reached 97.10**%,** while no recorded inundation occurred within the low and very low classes. This result should be interpreted as strong spatial agreement between the

modeled susceptibility surface and the available historical inundation record rather than as an absolute predictive accuracy value. The finding nevertheless strengthens confidence that the selected parameters are capturing the dominant physical conditions associated with observed flooding in the study area. The remaining 2.89% of historical inundation located within the moderate class also serves as an important reminder that local flooding may be influenced by factors not represented at the resolution of the model, including secondary drainage performance, localized sedimentation, culvert capacity, and temporary obstruction of drainage channels.

The validation pattern is broadly consistent with previous GEE-based flood studies in Indonesia. Irfan et al. (2025) demonstrated that flood mapping with Sentinel-1 imagery and GEE in Pekanbaru could be evaluated against recorded flood-event information, reinforcing the value of independent observational data when assessing satellite-based flood products. Pratama et al. (2024) likewise showed the utility of GEE for identifying hydrometeorological characteristics associated with flood occurrence in Kampar, while Saifurridzal & Sakinah (2022) demonstrated its usefulness for distinguishing flood-prone and relatively safer coastal zones. The present study differs from event-oriented flood detection because it does not treat a single satellite-derived inundation image as the susceptibility model itself. Six hydrological and geospatial parameters are first integrated into a persistent FSI surface, and historical inundation data are subsequently used as independent evidence of spatial correspondence. This distinction allows the resulting map to represent where physical conditions favor flooding beyond a single event or observation date.

The use of Google Earth Engine also contributes to the methodological value of the study. GEE provides access to multi-source Earth observation datasets and cloud-based computation within a common analytical environment, reducing the need to process each large raster dataset independently on local hardware (Gorelick et al., 2017). This advantage is particularly relevant to flood susceptibility analysis because rainfall, elevation, slope, soil, land cover, and hydrographic information originate from sources with different spatial and temporal characteristics. Bringing these datasets into a standardized workflow improves reproducibility and facilitates future updating when newer rainfall or land-cover data become available. The contribution of the present research therefore lies not simply in using GEE as a processing platform, but in connecting cloud-based geospatial analysis with hydrological reasoning at the sub-watershed scale.

The findings also have practical implications for disaster mitigation and spatial planning in Padang City. The concentration of very high susceptibility in the developed downstream zone suggests that flood management should not be confined to emergency response after inundation occurs. The resulting susceptibility map can support the prioritization of drainage improvement, river-corridor management, protection of remaining infiltration areas, evaluation of future development proposals, and identification of locations requiring more detailed hydrodynamic investigation. The map may also provide a spatial baseline for local institutions when integrating physical flood susceptibility with population, infrastructure, and socioeconomic data. Such integration is necessary before the analysis can be extended from a susceptibility assessment to a comprehensive flood-risk assessment. From this perspective, the FSI map is most useful as an evidence base for more informed decisions rather than as a final representation of all dimensions of disaster risk.

Several methodological constraints should be considered when interpreting these findings. The AHP weights represent a structured baseline based on the assumed relative importance of the six parameters; different expert judgments or watershed characteristics could produce different weighting structures. The spatial resolution of some source datasets also limits the level of detail that can be inferred. CHIRPS has a substantially coarser native resolution than the 30 m analysis grid, while OpenLandMap soil texture data are also coarser than the final grid. Resampling these datasets to 30 m enables geometric alignment among layers but does not create additional rainfall or soil information at that scale. Soil-texture gaps filled through neighboring modal classes should similarly be understood as spatial estimates rather than substitutes for field-based soil observations.

Uncertainty also arises from the automated river network derived from MERIT Hydro and the machine-learning-based Dynamic World land-cover classification. Extracted drainage paths may differ locally from river channels that have been modified through engineering works, sedimentation, or channel normalization, while land-cover transitions may be subject to classification uncertainty. The FSI itself represents relative physical susceptibility and does not simulate flood depth, flow velocity, inundation duration, or other outputs normally produced by hydrodynamic models. Social vulnerability, exposed population, infrastructure value, and institutional coping capacity were also outside the scope of the model, meaning that the resulting product should not be interpreted as a flood-risk map. Finally, the reported 97.10% spatial correspondence depends on the completeness and positional quality of historical inundation polygons available from Ina-Geoportal. Locations

that were flooded but not recorded in the reference database cannot contribute to the validation result. Future research would therefore benefit from combining higher-resolution rainfall observations, field-verified river geometry and soil information, multi-event satellite inundation records, and hydrodynamic modelling to evaluate the robustness of the susceptibility pattern under different flood scenarios.

CONCLUSION

Based on the research findings and discussion, the Batang Kandis Sub-watershed is characterized by a combination of biophysical conditions that strongly support the occurrence of flooding. The area receives high annual rainfall, averaging approximately 3,896 mm/year, while 80.44% of the terrain lies below 25 m above sea level and 63.61% has slopes of only 0–8%. These conditions are further reinforced by the dominance of clay loam and clay soils, which together cover more than 90% of the mapped soil area and have relatively low infiltration capacity, as well as by the substantial proportion of built-up land, which reaches 44.22% of the terrestrial area. Integration of these characteristics through Google Earth Engine and the AHP-based weighted overlay produced a Flood Susceptibility Index (FSI) in which rainfall received the highest weight of 25%, followed by river proximity and elevation at 20% each, slope at 15%, and soil texture and land cover at 10% each.

The resulting flood susceptibility map classified 58.77% of the study area as very highly susceptible and 21.39% as highly susceptible, meaning that more than 80% of the analyzed terrestrial area falls within the two upper susceptibility classes. These zones are concentrated mainly in the downstream and river-adjacent areas, where low elevation, gentle slopes, built-up surfaces, and accumulated runoff interact most strongly. Historical inundation data from Ina-Geoportal showed that 97.10% of the recorded flood area corresponded spatially with the high and very high susceptibility zones, indicating strong agreement between the modeled pattern and observed flood occurrence. The findings demonstrate that the integration of hydrological data, multi-source geospatial information, and cloud-based processing can provide a practical and spatially meaningful basis for flood mitigation, watershed management, and adaptive land-use planning in the Batang Kandis Sub-watershed. Future studies should incorporate higher-resolution rainfall and soil data, field-verified river geometry, hydrodynamic modelling, and socioeconomic vulnerability indicators to extend the present susceptibility assessment toward a more comprehensive flood-risk analysis.

REFERENCES

Akram, S., & Mushtaq, S. (2024). Environmental change and floods: The long-ignored effects of displacement on mental health. *Frontiers in Public Health, 12*, Article 1434123. https://doi.org/10.3389/fpubh.2024.1434123

Andayono, T., Mera, M., Junaidi, J., & Dalrino, D. (2024). Infiltration capacity based on soil geophysical constants using artificial infiltration in residential land. *Teknomekanik, 7*(2), 126–138. https://doi.org/10.24036/teknomekanik.v7i2.31372

Arsyad, S. (2010). *Konservasi tanah dan air*. IPB Press. https://repository.ipb.ac.id/handle/123456789/42667

Asdak, C. (2010). *Hidrologi dan pengelolaan daerah aliran sungai* (5th rev. ed.). Gadjah Mada University Press.

Badan Informasi Geospasial. (n.d.). *Ina-Geoportal*. Retrieved August 31, 2026, from https://tanahair.indonesia.go.id/portal-web/webmap

Badan Penanggulangan Bencana Daerah Kota Padang. (2025). *Data kejadian banjir Kota Padang* [Unpublished data set].

Barendrecht, M. H., Matanó, A., Mendoza, H., Weesie, R., Rohse, M., Koehler, J., de Ruiter, M., Garcia, M., Mazzoleni, M., & Aerts, J. C. J. H. (2024). Exploring drought-to-flood interactions and dynamics: A global case review. *WIREs Water, 11*(4), Article e1726. https://doi.org/10.1002/wat2.1726

Bumi, I. S., & Rezagama, A. (2023). Pemodelan banjir dua dimensi Sungai Seruyan dengan menggunakan aplikasi HEC-RAS. *Jurnal Inovasi Konstruksi, 2*(1), 11–19. https://doi.org/10.56911/jik.v2i1.36

Chow, V. T., Maidment, D. R., & Mays, L. W. (1988). *Applied hydrology*. McGraw-Hill.

Climate Hazards Center. (n.d.). *CHIRPS precipitation daily: Climate Hazards Center InfraRed Precipitation With Station Data (Version 2.0 Final)* [Data set]. Google Earth Engine Data Catalog. Retrieved August 31, 2026, from https://developers.google.com/earth-engine/datasets/catalog/UCSB-CHG_CHIRPS_DAILY

Creswell, J. W. (2014). *Research design: Qualitative, quantitative, and mixed methods approaches* (4th ed.). SAGE Publications.

European Space Agency. (n.d.-a). *Harmonized Sentinel-2 MSI: MultiSpectral Instrument, Level-2A surface reflectance* [Data set]. Google Earth Engine Data Catalog. Retrieved August 31, 2026, from https://developers.google.com/earth-engine/datasets/catalog/COPERNICUS_S2_SR_HARMONIZED

European Space Agency. (n.d.-b). *Sentinel-1 SAR GRD: C-band Synthetic Aperture Radar Ground Range Detected, log scaling* [Data set]. Google Earth Engine Data Catalog. Retrieved August 31, 2026, from https://developers.google.com/earth-engine/datasets/catalog/COPERNICUS_S1_GRD

Gorelick, N., Hancher, M., Dixon, M., Ilyushchenko, S., Thau, D., & Moore, R. (2017). Google Earth Engine: Planetary-scale geospatial analysis for everyone. *Remote Sensing of Environment, 202*, 18–27. https://doi.org/10.1016/j.rse.2017.06.031

Hengl, T. (2018). *Soil texture classes (USDA system) for six soil depths (0, 10, 30, 60, 100, and 200 cm) at 250 m* (Version 02) [Data set]. Zenodo. https://doi.org/10.5281/zenodo.1475451

Irfan, R., Sutikno, S., & Yusa, M. (2025). Analysis of flood occurrence in Pekanbaru City using Google Earth Engine. *Rekayasa Sipil, 19*(1), 27–31. https://doi.org/10.21776/ub.rekayasasipil.2025.019.01.4

Kodoatie, R. J., & Sjarief, R. (2010). *Tata ruang air*. Andi.

Kuswardhana, A. T., Hidayah, E., & Wiyono, R. U. A. (2023). Pemetaan geospasial risiko banjir di Sub-DAS Gunting, Jombang, Jawa Timur. *Rekayasa Sipil, 17*(1), 54–65. https://doi.org/10.21776/ub.rekayasasipil.2023.017.01.8

Nugroho, D. A., & Handayani, W. (2021). Kajian faktor penyebab banjir dalam perspektif wilayah sungai: Pembelajaran dari subsistem drainase Sungai Beringin. *Jurnal Pembangunan Wilayah dan Kota, 17*(2), 119–136. https://doi.org/10.14710/pwk.v17i2.33912

Nurpasari, F., & Febriamansyah, R. (2020). Study of the public perspectives on the problems of Batang Kuranji River Basin management in Padang City, West Sumatra, Indonesia. *IOP Conference Series: Earth and Environmental Science, 583*(1), Article 012036. https://doi.org/10.1088/1755-1315/583/1/012036

Pratama, D., Sutikno, S., & Yusa, M. (2024). Pemetaan daerah rawan ancaman banjir di area Kabupaten Kampar dengan menggunakan GEE (Google Earth Engine): Analysis of flood inundation areas in Kabupaten Kampar using GEE (Google Earth Engine). *Jurnal Saintis, 24*(1), 21–28. https://doi.org/10.25299/saintis.2024.vol24(01).15487

Saifurridzal, S., & Sakinah, W. (2022). Penentuan zona aman banjir di wilayah pesisir Kabupaten Jember dengan pemanfaatan Google Earth Engine. *Juvenil: Jurnal Ilmiah Kelautan dan Perikanan, 3*(1), 1–7. https://doi.org/10.21107/juvenil.v3i1.14889

Shah, A. A., Ullah, W., Khan, N. A., Khan, A., Alotaibi, B. A., Alam, E., & Ullah, A. (2025). Health and livelihood impacts of flood hazards on internally displaced persons in Pakistan. *International Journal of Disaster Risk Reduction, 119*, Article 105295. https://doi.org/10.1016/j.ijdrr.2025.105295

Sibandze, P., Kalumba, A. M., Aljaddani, A. H., Zhou, L., & Afuye, G. A. (2025). Geospatial mapping and meteorological flood risk assessment: A global research trend analysis. *Environmental Management, 75*(1), 137–154. https://doi.org/10.1007/s00267-024-02059-0

Sugandhi, N., & Rakuasa, H. (2023). Utilization of Geogle Earth Engine for flood hazard analysis in DKI Jakarta Province. *Jurnal Riset Multidisiplin dan Inovasi Teknologi, 1*(2), 40–49. https://doi.org/10.59653/jimat.v1i02.216

Tian, D., Wang, L., Liu, H., Cohen, S., & Shu, S. (2026). DeepSAR Flood Mapper: Global flood mapping on Google Earth Engine cloud platform using MLP deep learning model with Sentinel-1 SAR imagery and HAND topographic data. *GIScience & Remote Sensing, 63*(1), Article 2612306. https://doi.org/10.1080/15481603.2025.2612306

World Meteorological Organization. (2025). *State of the global climate 2024* (WMO-No. 1368). https://wmo.int/publication-series/state-of-global-climate/state-of-global-climate-2024